Journal of Solid State Chemistry **161,** 416–423 (2001)
doi:10.1006/jssc.2001.9357, available online at http://www.idealibrary.com on IDEAL®

Cation Effects on the Formation of the One-Dimensional Uranyl Iodates $A_2[(UO_2)_3(IO_3)_4O_2]$ (A = K, Rb, Tl) and $AE[(UO_2)_2(IO_3)_2O_2](H_2O)$ (AE = Sr, Ba, Pb)

Amanda C. Bean and Thomas E. Albrecht-Schmitt[1]

Department of Chemistry, Auburn University, Auburn, Alabama 36849

Received June 8, 2001; in revised form July 30, 2001; accepted August 9, 2001

The reactions of UO_3 and I_2O_5 with RbCl, TlCl, $SrCl_2$, or $Pb(NO_3)_2$ at 200°C for 3 days in aqueous media result in the formation of $A_2[(UO_2)_3(IO_3)_4O_2]$ (A = Rb (1), Tl (2)) and $AE[(UO_2)_2(IO_3)_2O_2](H_2O)$ (AE = Sr (3), Pb, (4)). Compounds 1 and 2 are isostructural with $K_2[(UO_2)_3(IO_3)_4O_2]$, which has been prepared by similar methods. These compounds are composed of $^1_\infty[(UO_2)_3(IO_3)_4O_2]^{2-}$ chains built from the edge-sharing of UO_7 pentagonal bipyramids and UO_6 octahedra. Compounds 3 and 4 are isostructural with $Ba[(UO_2)_2(IO_3)_2O_2](H_2O)$, consisting of one-dimensional $^1_\infty[(UO_2)_2(IO_3)_2O_2]^{2-}$ ribbons formed from the edge-sharing of distorted UO_7 pentagonal bipyramids. The iodate groups in these compounds adopt both bridging and monodentate binding modes and further serve to terminate the edges of the uranium oxide chains. The alkali metal, alkaline-earth metal, and main group cations separate the chains or ribbons in these compounds forming contacts with terminal oxygen atoms from the iodate ligands. Crystallographic data (193 K, Mo$K\alpha$, $\lambda = 0.71073$): 1, triclinic, space group $P\bar{1}$, $a = 7.0834(8)$ Å, $b = 7.8935(9)$ Å, $c = 9.092(1)$ Å, $\alpha = 91.741(2)°$, $\beta = 105.110(2)°$, $\gamma = 92.214(2)°$, $Z = 1$, $R(F) = 3.39\%$ for 134 parameters with 1978 reflections with $I > 2\sigma(I)$; 2, triclinic, space group $P\bar{1}$, $a = 7.0602(6)$ Å, $b = 7.9475(6)$ Å, $c = 9.0175(7)$ Å, $\alpha = 91.867(1)°$, $\beta = 105.595(1)°$, $\gamma = 91.577(1)°$, $Z = 1$, $R(F) = 3.12\%$ for 134 parameters with 2220 reflections with $I > 2\sigma(I)$; 3, monoclinic, space group $P2_1/c$, $a = 7.8140(5)$ Å, $b = 6.9425(4)$ Å, $c = 21.434(1)$, $\beta = 99.324(1)°$, $Z = 4$, $R(F) = 4.20\%$ for 164 parameters with 2533 reflections with $I > 2\sigma(I)$; 4, monoclinic, space group $P2_1/c$, $a = 7.8441(5)$ Å, $b = 6.9328(4)$ Å, $c = 21.340(1)$, $\beta = 99.062(1)°$, $Z = 4$, $R(F) = 3.37\%$ for 164 parameters with 1965 reflections with $I > 2\sigma(I)$.

INTRODUCTION

The formation of extended inorganic architectures in hydrothermal syntheses is governed in part by the structure-directing effects of counterions, even if these only form hydrogen-bonding or Coulombic interactions with the surrounding framework (1). The subtle influences of counterions are particularly profound in inorganic–organic hybrids of which zeolites are the most celebrated example (2). While the exact role of structure-directing counterions remains elusive, careful control of the size, charge, and geometry of these agents allows for the systematic investigations of hydrothermal syntheses (2–4). This is a particularly powerful form of chemical manipulation when it is combined with structurally flexible transition metals, lanthanides, and actinides as found in the formation of organically templated compounds of V (5–13), Fe (14–21), Co (22–25), Nb (26–29), and U (30–42). These effects can also be observed when polydentate ligands with variable binding modes are utilized in the preparation of new inorganic solids, as the coordination modes of these ligands are also influenced by templating agents (43–46).

Recent studies in our group have focused on the hydrothermal syntheses of uranyl iodate compounds that are a combination of several aspects of the aforementioned concepts. First, the uranyl centers can adopt three different coordination geometries giving rise to six-coordinate $[UO_2X_4]^{n-}$ octahedra, seven-coordinate $[UO_2X_5]^{n-}$ pentagonal bipyramids, and eight-coordinate $[UO_2X_6]^{n-}$ hexagonal bipyramids (47–49). Second, we have structurally characterized examples of monodentate, bridging, and a combination of chelating and bridging coordination modes for the iodate ligands to uranyl centers (43–45). Finally, we noted that changes in the size of alkali and alkaline-earth metal cations in these compounds have dramatic effects on the type of uranyl iodate network that forms (44, 45). Similar observations also have been made in the preparation of alkali metal actinide chalcophosphates such as $Cs_8U_5(P_3S_{10})(PS_4)_6$ (50), $K_{10}Th_3(P_2S_7)_4(PS_4)_2$ (50), $A_5An(PS_4)_3$ (A = K, Rb, Cs; An = Th,U) (50), $A_2ThP_3Se_9$ (A = K, Rb) (51), $Cs_4Th_2P_5Se_{17}$ (51), and $Rb_4U_4P_4Se_{26}$ (52). In the syntheses of these compounds, alkali metal cation substitutions can result in significant structural

[1]To whom correspondence should be addressed.

0022-4596/01 $35.00

changes including the chemical transformation of the chalcophosphate ligands themselves (50–52).

In the present study we wish to elucidate the role of structure-directing agents in the formation of one-dimensional uranyl iodate compounds with the general formulas $A_2[(UO_2)_3(IO_3)_4O_2]$ (A = K, Rb, Tl) and $AE[(UO_2)_2(IO_3)_2O_2](H_2O)$ (AE = Sr, Ba, Pb). In particular, we seek to deconvolute the effects of counterion size versus charge in these studies. Herein we report the hydrothermal syntheses, structural characterization, vibrational spectroscopy, and thermal behavior of $A_2[(UO_2)_3(IO_3)_4O_2]$ (A = Rb, Tl) and $AE[(UO_2)_2(IO_3)_2O_2](H_2O)$ (AE = Sr, Pb). The syntheses and characterization of $K_2[(UO_2)_3(IO_3)_4O_2]$ and $Ba[(UO_2)_2(IO_3)_2O_2](H_2O)$ were recently reported by our group (44).

EXPERIMENTAL

Syntheses

UO_3 (99.8%, Alfa-Aesar), I_2O_5 (98%, Alfa-Aesar), RbCl (99%, Alfa-Aesar), TlCl (99.9%, Alfa-Aesar), $SrCl_2 \cdot 6H_2O$ (99.0%, Alfa-Aesar), and $Pb(NO_3)_2$ (99.994%, Fischer) were used as received. Distilled and Millipore filtered water was used in all reactions. The resistance of the water was 18.2 MΩ. *While the UO_3 contains depleted U, standard precautions for handling radioactive materials should be followed.* All reactions were carried out using 1 mL of water in 23-mL PTFE-lined autoclaves with a reaction temperature of 200°C and duration of 72 h. After this period, the autoclaves were cooled at 9°C/h to 23°C. The mother liquors were then decanted from the crystals, which were subsequently washed with methanol, and allowed to dry. SEM/EDX analyses were performed using a JEOL 840/Link Isis instrument. Elemental percentages were calibrated against standards. Typical results are within 5% of the ratios determined from single-crystal X-ray diffraction experiments. IR spectra were collected on a Nicolet 5PC FT-IR spectrometer from KBr pellets.

$Rb_2[(UO_2)_3(IO_3)_4O_2]$ (**1**). Compound **1** was synthesized from UO_3 (286 mg, 1 mmol), I_2O_5 (334 mg, 1 mmol), and RbCl (242 mg, 2 mmol). The product consisted of a yellow solution over golden prisms. Yield, 423 mg (74% yield based on U). EDX analysis for $Rb_2[(UO_2)_3(IO_3)_4O_2]$ provided a Rb:U:I ratio of 2:3:4. IR (KBr, cm^{-1}): ν(U=O) 896 (s); ν(U=O, U–O, and I=O) 864 (b), 831 (s), 796 (m, sh), 786 (m, sh), 741 (s), 717 (s), 694 (s, b), 669 (m, sh), 501 (s), 443 (m) (53). DSC: 495°C (− 0.3720 W/g), 573°C (− 1.515 W/g), 586°C (− 1.280 W/g).

$Tl_2[(UO_2)_3(IO_3)_4O_2]$ (**2**). Compound **2** was synthesized from UO_3 (429 mg, 1.5 mmol), I_2O_5 (334 mg, 1 mmol), and TlCl (240 mg, 1 mmol). The product consisted of a yellow solution over deep orange elongated plates. Yield, 798 mg (82% yield based on U). EDX analysis for $Tl_2[(UO_2)_3(IO_3)_4O_2]$ provided a Tl:U:I ratio of 2:3:4. IR (KBr, cm^{-1}): ν(U=O) 904 (m, sh); ν(U=O, U–O, and I=O) 886 (s, b), 848 (m), 831 (m), 816 (s), 785 (m, b), 772 (m), 734 (s, sh), 714 (s, sh), 692 (s, br), 668 (s, sh), 490 (s, b), 442 (m, b), 424 (m, sh), 420 (m, sh) (53). DSC: 524°C (− 2.470 W/g).

$Sr[(UO_2)_2(IO_3)_2O_2](H_2O)$ (**3**). Compound **3** was synthesized from UO_3 (286 mg, 1 mmol), I_2O_5 (334 mg, 1 mmol), and $SrCl_2 \cdot 6H_2O$ (533 mg, 2 mmol). The product consisted of a yellow solution over golden prisms. Yield, 238 mg (44% yield based on U). EDX analysis for $Sr[(UO_2)_2(IO_3)_2O_2](H_2O)$ provided a Sr:U:I ratio of 1:2:2. IR (KBr, cm^{-1}): ν(U=O) 910 (m, sh); ν(U=O, U–O, and I=O) 846 (s), 831 (m, sh), 808 (w), 789 (m, sh), 779 (s), 722 (s, sh), 714 (s, sh), 582 (w), 523 (m), 461 (m, sh) (53). DSC: 274°C (− 0.490 W/g), 492°C (− 0.485 W/g), 565°C (− 1.321 W/g).

$Pb[(UO_2)_2(IO_3)_2O_2](H_2O)$ (**4**). Compound **4** was synthesized from UO_3 (429 mg, 1.5 mmol), I_2O_5 (334 mg, 1 mmol), and $Pb(NO_3)_2$ (331 mg, 1 mmol). The product consisted of a yellow solution over clusters of red-orange rectangular plates. Yield, 285 mg (36% yield based on U). EDX analysis for $Pb[(UO_2)_2(IO_3)_2O_2](H_2O)$ provided a Pb:U:I ratio of 1:2:2. IR (KBr, cm^{-1}): ν(U=O) 899 (m, sh); ν(U=O, U–O, and I=O) 838 (s), 808 (w, sh), 799 (m, sh), 778 (m), 758 (m), 722 (s, sh), 707 (s, sh), 595 (w), 563 (w), 520 (m), 458 (m, b) (53). DSC: 276°C (− 0.4647 W/g), 454°C (− 0.584 W/g), 496°C (− 0.580 W/g), 556°C (− 1.642 W/g).

Crystallographic Studies

Crystals of **1**, **2**, **3**, and **4** with the dimensions of 0.02 mm × 0.04 mm × 0.10 mm, 0.02 mm × 0.03 mm × 0.25 mm, 0.02 mm × 0.18 mm × 0.40 mm, and 0.02 mm × 0.04 mm × 0.28 mm, respectively, were mounted on glass fibers and aligned on a Bruker SMART APEX CCD X-ray diffractometer. Intensity measurements were performed using graphite monochromated Mo$K\alpha$ radiation from a sealed tube and a monocapillary. SMART was used for preliminary determination of the cell constants and data collection control. For all compounds, the intensities of reflections of a sphere were collected by a combination of three sets of exposures (frames). Each set had a different ϕ angle for the crystal and each exposure covered a range of 0.3° in ω. A total of 1800 frames were collected with an exposure time per frame of 30 s.

For **1**, **2**, **3**, and **4**, determination of integral intensities and global cell refinement were performed with the Bruker SAINT (v. 6.02) software package using a narrow-frame integration algorithm. A semi-empirical absorption correction was applied based on the intensities of symmetry-related reflections measured at different angular settings using SADABS for **1** and **3** (54). Owing to the very large absorption coefficients for **2** and **4**, analytical absorption

TABLE 1
Crystallographic Data for $Rb_2[(UO_2)_3(IO_3)_4O_2]$ (1) and $Tl_2[(UO_2)_3(IO_3)_4O_2]$ (2)

Formula	$Rb_2[(UO_2)_3(IO_3)_4O_2]$	$Tl_2[(UO_2)_3(IO_3)_4O_2]$
Formula mass (amu)	1712.63	1950.43
Space group	$P\bar{1}$ (No. 2)	$P\bar{1}$ (No. 2)
a (Å)	7.0834(8)	7.0602(6)
b (Å)	7.8935(9)	7.9475(6)
c (Å)	9.092(1)	9.0175(7)
α (deg.)	91.741(2)	91.867(1)
β (deg.)	105.110(2)	105.595(1)
γ (deg.)	92.214(2)	91.577(1)
V (Å^3)	490.0(1)	486.75(7)
Z	1	1
T (°C)	− 80	− 80
λ (Å)	0.710 73	0.710 73
ρ_{calcd} (g cm^{-3})	5.804	6.654
μ(Mo $K\alpha$) (cm^{-1})	360.56	478.01
$R(F)$ for $F_o^2 > 2\sigma(F_o^2)$[a]	0.0339	0.0312
$R_w(F_o^2)$[b]	0.0845	0.0849

[a] $R(F) = \sum \| F_o| - |F_c\| / \sum |F_o|$. [b] $R_w(F_o^2) = [\sum [w(F_o^2 - F_c^2)^2] / \sum wF_o^4]^{1/2}$.

TABLE 3
Atomic Coordinates and Equivalent Isotropic Displacement Parameters for $Rb_2[(UO_2)_3(IO_3)_4O_2]$ (1)

Atom	x	y	z	U_{eq}(Å^2)[a]
U(1)	0.4496(1)	0.0774(1)	− 0.1937(1)	0.010(1)
U(2)	0	0	0	0.014(1)
I(1)	0.8743(1)	0.1924(1)	− 0.3781(1)	0.013(1)
I(2)	0.2970(1)	0.3436(1)	− 0.5612(1)	0.014(1)
Rb(1)	0.2399(1)	0.5863(1)	− 0.1509(1)	0.023(1)
O(1)	0.7692(9)	0.0755(9)	− 0.2414(7)	0.020(1)
O(2)	0.1059(9)	0.1086(10)	− 0.2835(8)	0.029(2)
O(3)	0.8932(11)	0.3968(9)	− 0.2846(8)	0.028(2)
O(4)	0.0495(9)	0.2776(9)	− 0.5605(8)	0.025(2)
O(5)	0.3515(10)	0.5178(9)	− 0.4232(8)	0.023(2)
O(6)	0.4276(9)	0.1786(9)	− 0.4435(7)	0.020(1)
O(7)	0.6918(8)	0.0161(8)	0.0146(7)	0.015(1)
O(8)	0.4761(10)	0.2944(8)	− 0.1227(8)	0.019(1)
O(9)	0.4196(9)	-0.1353(8)	− 0.2737(8)	0.019(1)
O(10)	0.0491(10)	0.2175(9)	0.0651(9)	0.024(2)

[a] U_{eq} is defined as one-third of the trace of the orthogonalized $\mathbf{U}_{ij}$ tensor.

corrections were used in the place of SADABS. The program suite SHELXTL (v. 5.1) was used for space group determination (XPREP), structure solution (XS), and refinement (XL) (55). Heavy atoms dominate the X-ray scattering in $AE[(UO_2)_2(IO_3)_2O_2](H_2O)$ (AE = Sr, Pb) making the determination of hydrogen positions for the water molecule unreliable, and they were not included in the structural model. The final refinement included displacement parameters for all atoms and a secondary extinction parameter. Some crystallographic details are listed in Table 1 for **1** and **2**, and in Table 2 for **3** and **4**. The final positional parameters for **1**, **2**, **3**, and **4** are given in Tables 3, 4, 5, and 6, respectively. Additional crystallographic details are available from the author.

TABLE 2
Crystallographic Data for $Sr[(UO_2)_2(IO_3)_2O_2](H_2O)$ (3) and $Pb[(UO_2)_2(IO_3)_2O_2](H_2O)$ (4)

Formula	$Sr[(UO_2)_2(IO_3)_2O_2](H_2O)$	$Pb[(UO_2)_2(IO_3)_2O_2](H_2O)$
Formula mass (amu)	1027.50	1147.07
Space group	$P2_1/c$ (No. 14)	$P2_1/c$ (No. 14)
a (Å)	7.8140(5)	7.8441(5)
b (Å)	6.9425(4)	6.9328(4)
c (Å)	21.434(1)	21.340(1)
α (deg.)	90	90
β (deg.)	99.324(1)	99.062(1)
γ (deg.)	90	90
V (Å^3)	1147.4(1)	1146.0(1)
Z	4	4
T(°C)	− 80	− 80
λ (Å)	0.710 73	0.710 73
ρ_{calcd} (g cm^{-3})	5.936	6.637
μ(Mo $K\alpha$) (cm^{-1})	382.37	483.00
$R(F)$ for $F_o^2 > 2\sigma(F_o^2)$[a]	0.0420	0.0337
$R_w(F_o^2)$[b]	0.0979	0.0865

[a] $R(F) = \sum \| F_o| - |F_c\| / \sum |F_o|$. [b] $R_w(F_o^2) = [\sum [w(F_o^2 - F_c^2)^2] / \sum wF_o^4]^{1/2}$.

Differential Scanning Calorimetry Measurements

Thermal data for **1**, **2**, **3**, and **4** were collected using a TA Instruments Model 2920 differential scanning calorimeter (DSC). Samples (20 mg) were encapsulated in aluminum pans and heated at 10°C/min from 25°C to 600°C under a nitrogen atmosphere.

TABLE 4
Atomic Coordinates and Equivalent Isotropic Displacement Parameters for $Tl_2[(UO_2)_3(IO_3)_4O_2]$ (2)

Atom	x	y	z	U_{eq} (Å^2)[a]
U(1)	0.4475(1)	0.0761(1)	− 0.1966(1)	0.011(1)
U(2)	0	0	0	0.016(1)
I(1)	0.8731(1)	0.1948(1)	− 0.3812(1)	0.012(1)
I(2)	0.2923(1)	0.3471(1)	− 0.5653(1)	0.013(1)
Tl(1)	0.2442(1)	0.5903(1)	− 0.1569(1)	0.020(1)
O(1)	0.7696(10)	0.0858(10)	− 0.2408(8)	0.020(1)
O(2)	0.1049(10)	0.0973(10)	− 0.2938(9)	0.026(2)
O(3)	0.9092(12)	0.3953(10)	− 0.2814(9)	0.024(2)
O(4)	0.0450(10)	0.2843(10)	− 0.5652(8)	0.020(1)
O(5)	0.3487(10)	0.5205(9)	− 0.4261(8)	0.019(1)
O(6)	0.4218(10)	0.1834(9)	− 0.4473(8)	0.020(1)
O(7)	0.6912(9)	0.0186(8)	0.0145(7)	0.015(1)
O(8)	0.4628(10)	0.2906(9)	− 0.1252(8)	0.019(1)
O(9)	0.4272(10)	− 0.1367(8)	− 0.2771(8)	0.015(1)
O(10)	0.0543(10)	0.2145(9)	0.0737(9)	0.023(2)

TABLE 5
Atomic Coordinates and Equivalent Isotropic Displacement Parameters for $Sr[(UO_2)_2(IO_3)_2O_2](H_2O)$ (3)

Atom	x	y	z	U_{eq} (Å^2)[a]
U(1)	0.3905(1)	0.3276(1)	0.8764(1)	0.006(1)
U(2)	0.5225(1)	0.3025(1)	0.7204(1)	0.007(1)
I(1)	0.1642(1)	0.3168(1)	0.0298(1)	0.006(1)
I(2)	0.3027(1)	0.8249(1)	0.9509(1)	0.006(1)
Sr(1)	0.8667(1)	0.1200(2)	0.8666(1)	0.009(1)
O(1)	0.3195(10)	0.4045(10)	0.9814(3)	0.009(2)
O(2)	0.2188(10)	0.0647(10)	0.0345(3)	0.006(1)
O(3)	−0.0283(10)	0.3165(10)	0.9698(4)	0.010(2)
O(4)	0.3858(11)	0.6877(10)	0.8894(4)	0.011(2)
O(5)	0.4085(10)	0.0448(10)	0.9338(3)	0.011(2)
O(6)	0.0874(10)	0.8571(11)	0.9090(4)	0.012(2)
O(7)	0.6238(10)	0.3444(10)	0.9043(4)	0.009(2)
O(8)	0.1581(10)	0.3034(10)	0.8536(4)	0.011(2)
O(9)	0.4527(11)	0.1158(11)	0.8054(4)	0.013(2)
O(10)	0.7380(10)	0.3219(11)	0.7677(4)	0.011(2)
O(11)	0.3095(11)	0.2926(10)	0.6721(4)	0.012(2)
O(12)	0.4151(11)	0.4885(11)	0.7908(3)	0.010(2)
O(13)	0.9767(12)	0.0056(16)	0.7676(4)	0.031(2)

RESULTS AND DISCUSSION

Syntheses

The hydrothermal reactions of UO_3 with sources of IO_3^-, such as I_2O_5 and HIO_3 in the presence of alkali metal, alkaline-earth metal, and main group cations, yield one dimensional uranyl iodate compounds with two general structural motifs. Monovalent cations allow for the isolation of uranyl iodate compounds with the formula $A_2[(UO_2)_3(IO_3)_4O_2]$ (A = K (44), Rb, Tl) in yields ranging from 73–82%, depending on the cation employed (44). These solids are isolated as golden crystals that are easily distinguished from $UO_2(IO_3)_2$ and $UO_2(IO_3)_2(H_2O)$ on the basis of color and crystal habit (43). We have been unable to isolate the Cs^+ analogue of these aforementioned compounds, probably owing to its significantly larger size. Instead, a complex cesium uranyl chloroiodate, $Cs_2[(UO_2)_3Cl_2(IO_3)(OH)O_2]\cdot 2H_2O$, crystallizes from these hydrothermal reactions (56). Furthermore, reaction concentrations of RbCl in excess of 2 M lead to the formation of rubidium uranyl chloroiodates (56). These latter chloride-containing compounds do not form in supercritical water (425°C), but rather are only isolated when mild (200°C) hydrothermal conditions are employed.

When divalent cations, such as Sr^{2+}, Ba^{2+}, and Pb^{2+}, are used as counterions, $AE[(UO_2)_2(IO_3)_2O_2](H_2O)$ (AE = Sr, Ba (44), Pb) are isolated. These compounds form in lower amounts than those with monovalent cations, with isolated yields ranging from 36–60%. Rather than being due to solubility factors, this is apparently a thermal stability issue, due to the onset of decomposition beginning at approximately 275°C through the loss of water. Therefore, this phase is probably only available from mild hydrothermal reactions.

TABLE 6
Atomic Coordinates and Equivalent Isotropic Displacement Parameters for $Pb[(UO_2)_2(IO_3)_2O_2](H_2O)$ (4)

Atom	x	y	z	U_{eq}(Å^2)[a]
U(1)	0.3910(1)	0.3290(1)	0.8764(1)	0.009(1)
U(2)	0.5214(1)	0.3040(1)	0.7195(1)	0.009(1)
Pb(1)	0.8743(1)	0.1183(1)	0.8651(1)	0.014(1)
I(1)	0.1637(1)	0.3205(1)	0.0302(1)	0.008(1)
I(2)	0.3013(1)	0.8290(1)	0.9508(1)	0.009(1)
O(1)	0.3138(9)	0.4110(10)	0.9802(3)	0.013(2)
O(2)	0.2187(9)	0.0671(9)	0.0346(4)	0.012(2)
O(3)	−0.0317(10)	0.3183(9)	0.9720(4)	0.015(2)
O(4)	0.3866(10)	0.6919(10)	0.8897(4)	0.015(2)
O(5)	0.4112(9)	0.0489(9)	0.9340(3)	0.013(2)
O(6)	0.0880(10)	0.8612(11)	0.9074(4)	0.016(2)
O(7)	0.6194(10)	0.3519(10)	0.9066(4)	0.012(2)
O(8)	0.1594(10)	0.3002(9)	0.8519(4)	0.012(2)
O(9)	0.4576(9)	0.1184(10)	0.8063(3)	0.012(2)
O(10)	0.7382(10)	0.3266(10)	0.7635(4)	0.013(2)
O(11)	0.3058(10)	0.2900(9)	0.6731(3)	0.010(2)
O(12)	0.4151(9)	0.4886(10)	0.7901(3)	0.011(2)
O(13)	0.9734(11)	0.0094(14)	0.7658(4)	0.033(2)

Structures

$A_2[(UO_2)_3(IO_3)_4O_2]$ ($A = Rb$ (**1**), Tl (**2**)). Compounds **1** and **2** are isostructural with $K_2[(UO_2)_3(IO_3)_4O_2]$ (44), which was recently reported by our group. $A_2[(UO_2)_3(IO_3)_4O_2]$ (A = K, Rb, Tl) consists of infinite one-dimensional $^1_\infty[(UO_2)_3(IO_3)_4O_2]^{2-}$ chains that run down the a-axis. These chains are constructed from UO_7 pentagonal bipyramids and UO_6 octahedra. The UO_7 polyhedra edge-share to form dimers that are linked together by UO_6 octahedra. The edges of the uranium oxide chains are terminated by iodate anions that adopt both bridging and monodentate binding modes. The bridging iodates join the dimers of edge-sharing UO_7 pentagonal bipyramids and form two opposite corners of the distorted UO_6 octahedra. The coordination polyhedra of the uranium atoms are completed by μ_3-O^{2-} ligands that are shared by both the dimers of edge-sharing UO_7 pentagonal bipyramids and the UO_6 octahedra. Part of one of these uranyl iodate chains is shown in Fig. 1a. A polyhedral illustration of this chain is depicted in Fig. 1b. The A^+ (A = Rb, Tl) cations separate the chains from one another and are coordinated by terminal oxygen atoms from iodate ligands. These cations are coordinated by eight oxygen atoms from the iodate ligands in a bicapped trigonal prismatic geometry. The

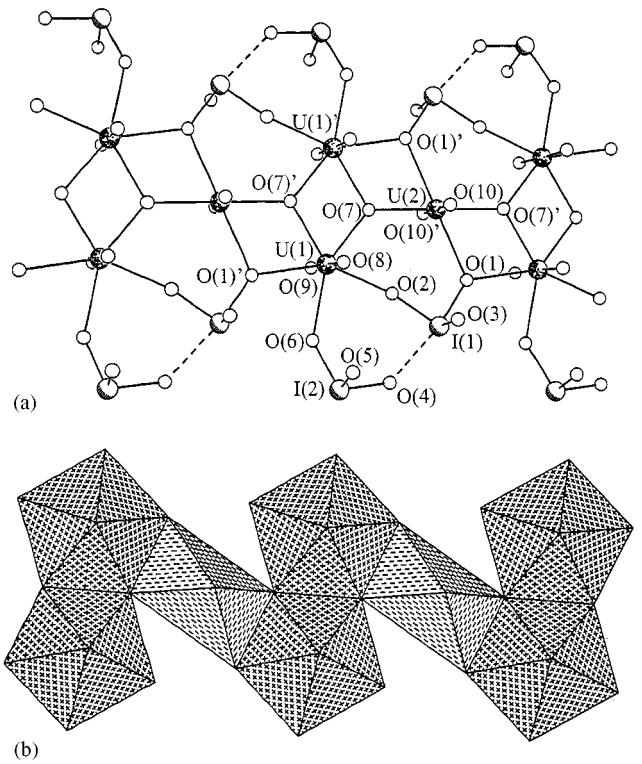

FIG. 1. (a) Infinite one-dimensional $^{1}_{\infty}[(UO_2)_3(IO_3)_4O_2]^{2-}$ chains constructed from dimers of edge-sharing UO_7 pentagonal bipyramids that are linked together with distorted UO_6 octahedra running down the *a*-axis in $A_2[(UO_2)_3(IO_3)_4O_2]$ (A = Rb, Tl). (b) A polyhedral representation of the one-dimensional uranium oxide chains in $A_2[(UO_2)_3(IO_3)_4O_2]$ (A = Rb, Tl).

capping of the prism occurs on one rectangular face and on one of the ends of the trigonal prism. A depiction of the complete structure of **1** and **2**, viewed down the *a*-axis, is shown in Fig. 2.

The U=O bond lengths for the UO_6 polyhedra are 1.790(7) ($\times 2$) and 1.802(7) ($\times 2$) Å for **1** and **2**. These bonds are similar to those found in the UO_7 units, which have U=O bond lengths of 1.798(6) and 1.792(6) Å for **1** and 1.793(7) and 1.805(7) Å for **2**. The remaining equatorial ligands show significant variations with U–O distances ranging from 2.251(6) to 2.414(6) Å and 2.264(6) to 2.412(7) Å for the UO_7 pentagonal bipyramids in **1** and **2**, respectively. The UO_6 octahedra are also highly distorted with equatorial U–O bond lengths of 2.476(6) ($\times 2$) and 2.230(5) ($\times 2$) for **1** and 2.466(7) ($\times 2$) and 2.228(6) ($\times 2$) for **2**. These distortions are due to differences in the coordination of the iodate anions to the uranyl moieties versus coordination by oxide, with the former representing the long bonds and the latter being the short bonds.

The iodate ligands show I=O bond length variations consistent with their mode of coordination to the uranium centers. The bridging iodate anion shows the most significant deviation from C_{3v} symmetry with the μ_3-O(1) atom showing the longest I=O bond distance of 1.857(6) and 1.850(6) Å in **1** and **2**. The other I=O bond lengths of 1.803(6) and 1.785(7) Å for **1** and 1.821(7) and 1.782(8) Å for **2** are similar to those found for the monodentate iodate anions which have bond distances ranging from 1.793(7) to 1.833(6) Å for **1** and 1.795(7) to 1.815(6) Å for **2**. As found in many iodate compounds including $UO_2(IO_3)_2$ and $UO_2(IO_3)_2(H_2O)$ (43), there are close I $\cdots$ O contacts of 2.413(6) and 2.417(7) Å for **1** and **2** between the terminal oxygen atoms from the monodentate iodate ligand and the neighboring iodine atom from the iodate that bridges uranium centers. The most significant differences between $K_2[(UO_2)_3(IO_3)_4O_2]$ and **1** and **2** are the *A*–O (A = Rb, Tl) contacts which range from 2.792(7) to 3.310(7) Å for **1** and 2.741(8) to 3.297(8) Å for **2**. These bond distances are approximately 0.1 Å longer than those found in $K_2[(UO_2)_3(IO_3)_4O_2]$. Selected bond lengths for **1** and **2** are given in Tables 7 and 8. Bond valence sum calculations provide values of 6.066 and 5.817 for **1** and 6.067 and 5.768 in **2** for U(1) and U(2), respectively (57, 58). Parameters for seven- and six-coordinate U(VI) from Burns *et al.* were used in this calculation (47).

AE$[(UO_2)_2(IO_3)_2O_2](H_2O)$ (*AE* = *Sr* (**3**), *Pb* (**4**)). Compounds **3** and **4** are isostructural with $Ba[(UO_2)_2(IO_3)_2O_2](H_2O)$ (44) and consist of edge-sharing distorted pentagonal bipyramidal UO_7 units that form one-dimensional uranium oxide ribbons whose edges are terminated by iodate ligands as shown in Fig. 3a. These ribbons run down the *b*-axis and are separated by the AE^{2+} (*AE* = Sr, Ba, Pb) cations and water molecules. The pentagonal

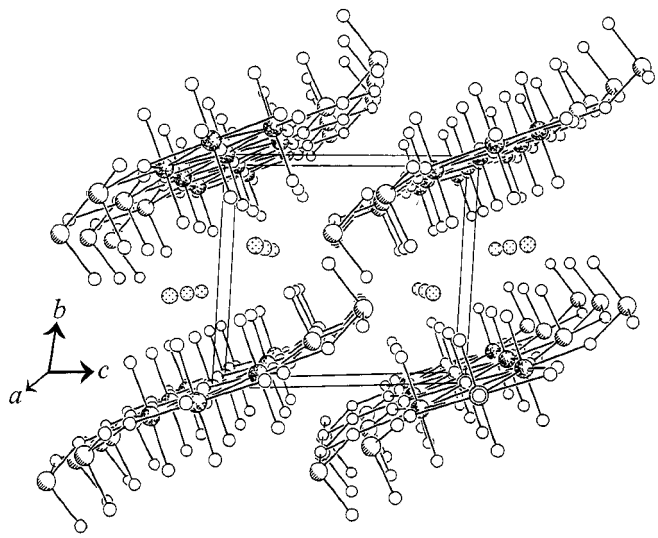

FIG. 2. A depiction of the structure of $A_2[(UO_2)_3(IO_3)_4O_2]$ (A = Rb, Tl) viewed down the *a*-axis.

TABLE 7
Selected Bond Distances (Å) for $Rb_2[(UO_2)_3(IO_3)_4O_2]$ (1)

U(1)–O(1)	2.414(6)	I(2)–O(4)	1.811(6)
U(1)–O(2)	2.383(6)	I(2)–O(5)	1.793(7)
U(1)–O(6)	2.399(6)	I(2)–O(6)	1.833(6)
U(1)–O(7)	2.278(6)	I(1)···O(4)	2.413(6)
U(1)–O(7)′	2.251(6)	Rb(1)–O(3)	2.792(7)
U(1)–O(8) (U = O)	1.798(6)	Rb(1)–O(4)	3.127(6)
U(1)–O(9) (U = O)	1.792(6)	Rb(1)–O(5)	2.831(7)
U(2)–O(1)	2.476(6) (×2)	Rb(1)–O(7)	3.310(7)
U(2)–O(7)	2.230(5) (×2)	Rb(1)–O(8)	2.878(7)
U(2)–O(10) (U = O)	1.790(7) (×2)	Rb(1)–O(8)′	2.868(7)
I(1)–O(1)	1.857(6)	Rb(1)–O(9)	2.893(7)
I(1)–O(2)	1.803(6)	Rb(1)–O(10)	2.864(7)
I(1)–O(3)	1.785(7)		

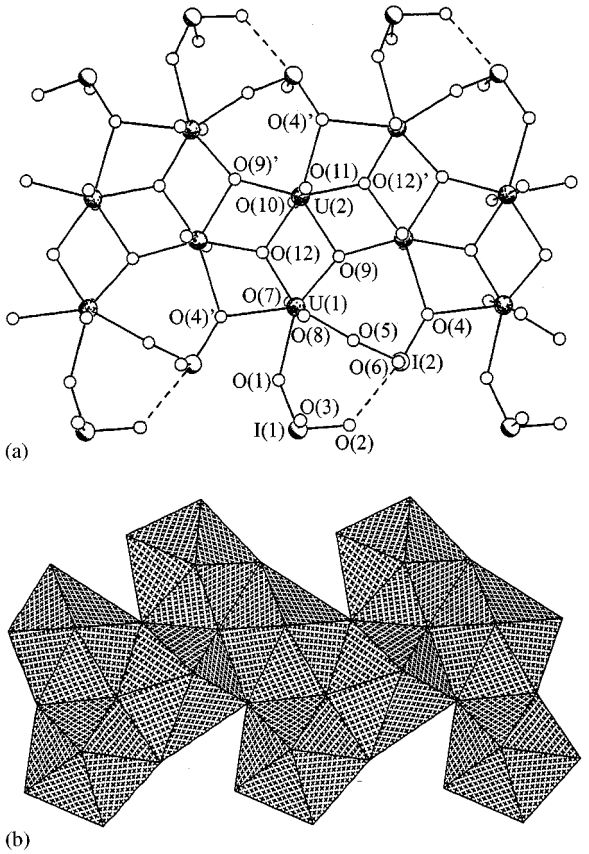

FIG. 3. (a) One-dimensional $^1_\infty[(UO_2)_2(IO_3)_2O_2]^{2-}$ ribbons in the structure of $AE[(UO_2)_2(IO_3)_2O_2](H_2O)$ (AE = Sr, Pb) consisting of edge-sharing distorted pentagonal bipyramidal UO_7 units. (b) A polyhedral representation of the one-dimensional uranium oxide ribbons built from edge-sharing distorted pentagonal bipyramids in $AE[(UO_2)_2(IO_3)_2O_2](H_2O)$ (AE = Sr, Pb).

bipyramids containing U(1) share two edges with neighboring polyhedra, and these units line the edges of the ribbons, whereas the pentagonal bipyramids containing U(2) are on the interior of the ribbons and share four edges with neighboring polyhedra as shown in Fig. 3b. As found in $A_2[(UO_2)_3(IO_3)_4O_2]$ (A = K, Rb, Tl), the iodate ligands adopt both monodentate and bridging binding modes and terminate the edges of the uranium oxide ribbons. The AE^{2+} cations are contained within distorted tricapped trigonal prisms where two rectangular faces and one triangular face are capped. Again, the longest distances of 3.289(8) Å in **3** and 3.311(8) Å in **4** are to the oxygen atom capping the triangular face. A complete illustration of the $AE[(UO_2)_2(IO_3)_2O_2](H_2O)$ (AE = Sr, Ba, Pb) structure is shown in Fig. 4. The structures of **3** and **4** represent significant improvements over that of $Ba[(UO_2)_2(IO_3)_2O_2](H_2O)$, which was solved from a twinned crystal (44).

The U=O bond lengths range from 1.813(8) to 1.828(8) Å for **3** and 1.813(8) to 1.823(7) Å for **4**, and are within expected ranges for uranyl moieties. The large distortions in the pentagonal plane of the two uranium centers in compounds **3** and **4** are due to differences in the coordination by the oxygen atoms from the iodate ligands when compared to coordination by the μ_3-oxide atoms. In these compounds the short U–O distances of approximately 2.2 Å are with the μ_3-oxide atoms and the longest bonds of approximately

TABLE 8
Selected Bond Distances (Å) for $Tl_2[(UO_2)_3(IO_3)_4O_2]$ (2)

U(1)–O(1)	2.412(7)	I(2)–O(4)	1.803(7)
U(1)–O(2)	2.354(7)	I(2)–O(5)	1.795(7)
U(1)–O(6)	2.405(6)	I(2)–O(6)	1.815(6)
U(1)–O(7)′	2.265(6)	I(1)···O(4)	2.417(7)
U(1)–O(7)	2.264(6)	Tl(1)–O(3)	2.741(8)
U(1)–O(8) (U = O)	1.793(7)	Tl(1)–O(4)	2.994(7)
U(1)–O(9) (U = O)	1.805(7)	Tl(1)–O(5)	2.765(7)
U(2)–O(1)	2.466(7) (×2)	Tl(1)–O(7)	3.297(8)
U(2)–O(7)	2.228(6) (×2)	Tl(1)–O(8)	2.924(7)
U(2)–O(10) (U = O)	1.802(7) (×2)	Tl(1)–O(8)′	2.854(7)
I(1)–O(1)	1.850(6)	Tl(1)–O(9)	2.882(7)
I(1)–O(2)	1.821(7)	Tl(1)–O(10)	2.892(7)
I(1)–O(3)	1.782(8)		

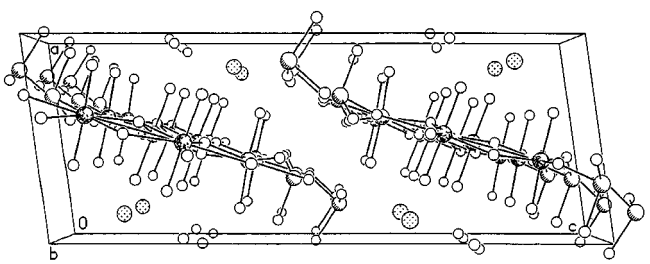

FIG. 4. An illustration of the structure of $AE[(UO_2)_2(IO_3)_2O_2](H_2O)$ (AE = Sr, Pb) viewed down the b-axis.

TABLE 9
Selected Bond Distances (Å) for $Sr[(UO_2)_2(IO_3)_2O_2](H_2O)$ (3)

U(1)–O(1)	2.462(7)	I(1)–O(2)	1.800(7)
U(1)–O(4)	2.516(7)	I(1)–O(3)	1.813(8)
U(1)–O(5)	2.309(7)	I(2)–O(4)	1.829(8)
U(1)-O(7) (U = O)	1.828(8)	I(2)–O(5)	1.802(8)
U(1)-O(8) (U = O)	1.810(8)	I(2)–O(6)	1.788(8)
U(1)–O(9)	2.226(8)	I(2) ··· O(2)′	2.605(8)
U(1)–O(12)	2.183(7)	Sr(1)–O(2)	2.654(8)
U(2)–O(4)	2.689(8)	Sr(1)–O(3)	2.615(8)
U(2)–O(9)	2.371(8)	Sr(1)–O(6)	2.573(8)
U(2)–O(9)′	2.260(8)	Sr(1)–O(7)	2.679(8)
U(2)–O(10)	1.825(8)	Sr(1)–O(8)	2.663(8)
U(2)–O(11)	1.813(8)	Sr(1)–O(9)	3.289(8)
U(2)–O(12)	2.250(7)	Sr(1)–O(10)	2.604(8)
U(2)–O(12)′	2.255(7)	Sr(1)–O(11)	2.717(8)
I(1)–O(1)	1.824(7)	Sr(1)–O(13)	2.542(9)

2.6 Å are with the oxo groups from the iodate ligands. Typical I = O bond distances are found in **3** and **4** and range from 1.788(8) to 1.829(8) Å and 1.794(8) to 1.823(7) Å, respectively. As in $A_2[(UO_2)_3(IO_3)_4O_2]$ (A = K, Rb, Tl), there are I ··· O contacts; however, these are approximately 0.2 Å longer with distances of 2.605(8) and 2.591(8) Å between the terminal oxygen atoms from the monodentate iodate ligand and the neighboring iodine atom from the iodate that bridges uranium centers. *AE*–O (*AE* = Sr, Pb) contacts range from 2.542(9) to 3.289(8) Å for **3** and 2.515(7) to 3.311(8) Å for **4**. The shortest *AE*–O bonds are to the bound water molecules. Bond valence sum calculations provide values of 6.014 and 5.914, and 6.068 and 5.950, for U(1) and U(2) in **3** and **4**, respectively (57, 58). Parameters for seven-coordinate U(VI) from Burns *et al.* were used in this calculation (47). Selected bond lengths for **3** and **4** are given in Tables 9 and 10.

TABLE 10
Selected Bond Distances (Å) for $Pb[(UO_2)_2(IO_3)_2O_2](H_2O)$ (4)

U(1)–O(1)	2.454(7)	I(1)–O(2)	1.807(7)
U(1)–O(4)	2.533(7)	I(1)–O(3)	1.815(8)
U(1)–O(5)	2.291(7)	I(2)–O(4)	1.823(7)
U(1)-O(7) (U = O)	1.813(8)	I(2)–O(5)	1.814(7)
U(1)-O(8) (U = O)	1.820(8)	I(2)–O(6)	1.794(8)
U(1)–O(9)	2.211(7)	I(2) ··· O(2)′	2.591(8)
U(1)–O(12)	2.181(7)	Pb(1)–O(2)	2.694(7)
U(2)–O(4)	2.662(8)	Pb(1)–O(3)	2.673(8)
U(2)–O(9)	2.373(7)	Pb(1)–O(6)	2.515(7)
U(2)–O(9)′	2.260(7)	Pb(1)–O(7)	2.822(8)
U(2)–O(10)	1.815(8)	Pb(1)–O(8)	2.621(7)
U(2)–O(11)	1.823(7)	Pb(1)–O(9)	3.311(8)
U(2)–O(12)	2.236(7)	Pb(1)–O(10)	2.683(7)
U(2)–O(12)′	2.259(7)	Pb(1)–O(11)	2.734(7)
I(1)–O(1)	1.821(7)	Pb(1)–O(13)	2.487(8)

CONCLUSIONS

This systematic study on the effects of changes in cation size and charge on the formation of one-dimensional uranyl iodate compounds was inspired by our initial observation of the substantial differences in the structures of $K_2[(UO_2)_3(IO_3)_4O_2]$ and $Ba[(UO_2)_2(IO_3)_2O_2](H_2O)$. As we have reported in this study, K^+, Rb^+, and Tl^+ cations all yield isostructural compounds with the general formula $A_2[(UO_2)_3(IO_3)_4O_2]$. These eight-coordinate cations vary in size from 1.65 Å for K^+ to 1.73 Å for Tl^+ to 1.75 Å for Rb^+ (59). Therefore, small changes in cation size do not affect the structural chemistry of these compounds. We have been unable to isolate the Cs^+ analogue of these compounds, and have instead discovered a mixed-anion chloroiodate, $Cs_2[(UO_2)_3Cl_2(IO_3)(OH)O_2]\cdot 2H_2O$, which along with other compounds of this type, will be the subject of a future report (56). The dramatically increased size of this cation (1.90 Å) may be responsible for the substantial differences in this chemistry. While the nine-coordinate Ba^{2+} cation (1.61 Å) (59) is actually quite similar in size to K^+, compounds with the general formula $AE[(UO_2)_2(IO_3)_2O_2](H_2O)$ are isolated with Sr^{2+}, Ba^{2+}, and Pb^{2+}. The Sr^{2+} and Pb^{2+} dications are substantially smaller than Ba^{2+} with ionic radii of 1.45 and 1.49 Å (59). We can therefore conclude that within the size range of cations studied, charge plays a more substantial role than size in directing the formation of uranyl iodate compounds.

ACKNOWLEDGMENTS

This work was supported by NASA (Alabama Space Grant Consortium) and Auburn University.

REFERENCES

1. A. K. Cheetham, G. Férey, and T. Loiseau, *Angew. Chem., Int. Ed.* **38,** 3268 (1999).
2. M. E. Davis and R. F. Lobo, *Chem. Mater.* **4,** 756 (1992).
3. A. Rabenau, *Angew. Chem., Int. Ed. Engl.* **24,** 1026 (1985).
4. J. W. Kolis and M. B. Korzenski, *in* "Chemical Synthesis Using Supercritical Fluids" (P. G. Jessop and W. Leitner, Eds.), pp. 213–241. Wiley-VCH, New York, 1999.
5. R. C. Haushalter and L. A. Mundi, *Chem. Mater.* **4,** 31 (1992).
6. V. Soghomonian, R. Haushalter, Q. Chen, J. Zubieta, C. J. O'Connor, and Y.-S. Lee, *Chem. Mater.* **5,** 1690 (1993).
7. V. Soghomonian, Q. Chen, R. Haushalter, J. Zubieta, and C. J. O'Connor, *Science* **259,** 1596 (1993).
8. V. Soghomonian, Q. Chen, R. Haushalter, and J. Zubieta, *Angew. Chem., Int. Ed. Engl.* **32,** 610 (1993).
9. V. Soghomonian, R. Haushalter, Q. Chen, and J. Zubieta, *Inorg. Chem.* **33,** 1700 (1994).
10. M. I. Khan, Y.-S. Lee, C. J. O'Connor, R. C. Haushalter, and J. Zubieta, *Inorg. Chem.* **33**, 3855 (1994).
11. Y. Zhang, A. Clearfield, and R. C. Haushalter, *J. Solid State Chem.* **117,** 157 (1995).

12. Y. Zhang, A. Clearfield, and R. C. Haushalter, *Chem. Mater*. **7,** 1221 (1995).
13. M. E. Welk, A. J. Norquist, C. L. Stern, and K. R. Poeppelmeier, *Inorg. Chem.* **39,** 3946 (2000).
14. D. R. Corbin, J. F. Whitney, W. C. Fultz, G. D. Stucky, M. M. Eddy, and A. K. Cheetham, *Inorg. Chem.* **25,** 2279 (1986).
15. P. Feng, X. Bu, and G. D. Stucky, *Nature* **388,** 735 (1997).
16. A. Choudhury, S. Natarajan, and C. N. R. Rao, *Chem. Mater*. **11,** 2316 (1999).
17. M. Riou-Cavellec, C. Serre, J. Robino, M. Noguès, J.-M. Grenèche, and G. Férey, *J. Solid State Chem.* **147,** 122 (1999).
18. M. B. Korzenski, G. L. Schimek, and J. W. Kolis, *J. Solid State Chem.* **139,** 152 (1998).
19. M. B. Korzenski and J. W. Kolis, *J. Solid State Chem.* **147,** 390 (1999).
20. V. Zima, K.-H. Lii, N. Nguyen, and A. Ducouret, *Chem. Mater*. **10,** 1914 (1998).
21. M. Riou-Cavellec, D. Riou, and G. Férey, *Inorg. Chim. Acta* **291,** 317 (1999).
22. P. Feng, X. Bu, and G. D. Stucky, *J. Solid State Chem.* **129,** 328 (1997).
23. P. Feng, X. Bu, and G. D. Stucky, *J. Solid State Chem.* **131,** 160 (1997).
24. P. Feng, X. Bu, S. H. Tolbert, and G. D. Stucky, *J. Am. Chem. Soc*. **119,** 2497 (1997).
25. S.-Y. Mao, Y.-X. Huang, Z.-B. Wei, J.-X. Mi, Z.-L. Huang, and J.-T. Zhao, *J. Solid State Chem.* **149,** 292 (2000).
26. V. A. Sarin, V. Y. Dudarev, L. E. Fykin, Y. E. Gorbunova, E. G. Il'in, and Y. B. Buslaev, *Dokl. Akad. Nauk SSSR* **236,** 393 (1977).
27. P. S. Halasyamani, M. J. Willis, P. M. Lundquist, C. L. Stern, G. K. Wong, and K. R. Poeppelmeier, *Inorg. Chem.* **35,** 1367 (1996).
28. P. S. Halasyamani, K. R. Heier, M. J. Willis, C. L. Stern, and K. R. Poeppelmeier, *Anorg. Allg. Chem.* **622,** 479 (1996).
29. A. J. Norquist, C. L. Stern, and K. R. Poeppelmeier, *Inorg. Chem.* **38,** 3448 (1999).
30. P. M. Almond, C. E. Talley, A. C. Bean, S. M. Peper, and T. E. Albrecht-Schmitt, *J. Solid State Chem.* **154,** 635 (2000).
31. C. E. Talley, A. C. Bean, and T. E. Albrecht-Schmitt, *Inorg. Chem.* **39,** 5174 (2000).
32. R. J. Francis, P. S. Halasyamani, and D. O'Hare, *Angew. Chem., Int. Ed. Engl*. **37,** 2214 (1998).
33. R. J. Francis, P. S. Halasyamani, and D. O'Hare, *Chem. Mater*. **10,** 3131 (1998).
34. S. Allen, S. Barlow, P. S. Halasyamani, J. F. W. Mosselmans, D. O'Hare, S. M. Walker, and R. I. Walton, *Inorg. Chem.* **39,** 3791 (2000).
35. P. M. Almond, L. Deakin, M. J. Porter, A. Mar, and T. E. Albrecht-Schmitt, *Chem. Mater*. **12,** 3208 (2000).
36. P. M. Almond, L. Deakin, A. Mar, and T. E. Albrecht-Schmitt, *Inorg. Chem.* **40,** 886 (2001).
37. P. M. Almond, L. Deakin, A. Mar, and T. E. Albrecht-Schmitt, *J. Solid State Chem.* **158,** 87 (2001).
38. P. S. Halasyamani, S. M. Walker, and D. O'Hare, *J. Am. Chem. Soc*. **121,** 7415 (1999).
39. S. M. Walker, P. S. Halasyamani, S. Allen, and D. O'Hare, *J. Am. Chem. Soc*. **121,** 10513 (1999).
40. R. J. Francis, P. S. Halasyamani, J. S. Bee, and D. O'Hare, *J. Am. Chem. Soc*. **121,** 1609 (1999).
41. R. J. Francis, M. J. Drewitt, P. S. Halasyamani, C. Ranganathachar, D. O'Hare, W. Clegg, and S. J. Teat, *Chem. Commun*. **2,** 279 (1998).
42. P. S. Halasyamani, R. J. Francis, S. M. Walker, and D. O'Hare, *Inorg. Chem.* **38,** 271 (1999).
43. A. C. Bean, S. M. Peper, and T. E. Albrecht-Schmitt, *Chem. Mater*. **13,** 1266 (2001).
44. A. C. Bean, M. Ruf, and T. E. Albrecht-Schmitt, *Inorg. Chem.* **40,** 3959.
45. A. C. Bean, C. F. Campana, and T. E. Albrecht-Schmitt, *J. Am. Chem. Soc*., in press (2001).
46. C. R. Evenson IV and P. K. Dorhout, *Inorg. Chem.* **40,** 2884 (2001).
47. P. C. Burns, R. C. Ewing, and F. C. Hawthorne, *Can. Mineral*. **35,** 1551 (1997).
48. P. C. Burns, *In* "Uranium: Mineralogy, Geochemistry and the Environment" (P. C. Burns and R. Finch, Eds.), Chap. 1, Mineralogical Society of America, Washington, DC, 1999.
49. P. C. Burns, M. L. Miller, and R. C. Ewing, *Can. Mineral*. **34,** 845 (1996).
50. R. F. Hess, K. D. Abney, J. L. Burris, H. D. Hochheimer, and P. K. Dorhout, *Inorg. Chem.* **40,** 2851 (2001).
51. P. M. Briggs Piccoli, K. D. Abney, J. R. Schoonover, and P. K. Dorhout, *Inorg. Chem.* **39,** 2970 (2000).
52. K. Chondroudis and M. G. Kanatzidis, *J. Am. Chem. Soc*. **119,** 2574 (1997).
53. (a) A. Y. Tsivadze, N. N. Krot, and B. I. Muchnik, *Proc. Moscow Symp. Chem. Transuranium Elem.* 89 (1976); (b) A. Y. Tsivadze, B. I. Muchnik, and N. N. Krot, *Zh. Neorg. Khim.* 17, 3324 (1972).
54. *SADABS*, Program for absorption correction using SMART CCD based on the method of Blessing: Blessing, R. H. *Acta Crystallogr. A* **51,** 33 (1995).
55. G. M. Sheldrick, SHELXTL PC, Version 5.0, An Integrated System for Solving, Refining, and Displaying Crystal Structures from Diffraction Data; Siemens Analytical X-Ray Instruments, Inc., Madison, WI, 1994.
56. A. C. Bean, W. Runde, and T. E. Albrecht-Schmitt, *Inorg. Chem*., manuscript in preparation (2001).
57. I. D. Brown and D. Altermatt, *Acta Crystallogr. B* **41,** 244 (1985).
58. N. E. Brese and M. O'Keeffe, *Acta Crystallogr. B* **47,** 192 (1991).
59. R. D. Shannon, *Acta Crystallogr. A* **32,** 751 (1976).